High performance MRI simulation of arbitrarily complex flow: A versatile framework

Alexandre Fortin, Stéphanie Salmon, Joseph Baruthio, Maya Delbany, Emmanuel Durand

High performance MRI simulation of arbitrarily complex flow: A versatile framework

Fortin A.[a], Salmon S.[a], Baruthio J.[b], Delbany M.[b], Durand E.[c]

[a] *LMR, University of Reims Champagne-Ardenne, FR 3399, CNRS, France*
[b] *ICube, University of Strasbourg, UMR 7357, CNRS, FMTS, France*
[c] *IR4M, University Paris-Sud, UMR 8081, CNRS, France*

Abstract

PURPOSE: During the last decades, magnetic resonance angiography has been used as a clinical routine for precise and non-invasive exploration of vessels, as well as for diagnosis of the most current neurovascular diseases. Several dedicated codes were developed to simulate specifically the process of arbitrarily complex flow imaging. Though, currently, most of advanced MRI simulators do not include this option and are specialized in static tissues imaging. This work was carried out to expand the possibilities of one of those simulators in order to propose a complete full-featured tool for simulation of any MR experience including flow motion.

THEORY AND METHODS: An extension of JEMRIS, one of the most prevalent high performance open-source software for MRI simulation to date, is presented. Implementing a Lagrangian description of individual spins motion in the code makes possible to simulate any MR experience including both static tissues and arbitrarily complex flow.

RESULTS: The efficiency of this approach is proven by replicating some specific angiographic pulse sequences, such as phase contrast velocimetry, time-of-flight sequence and contrast-enhanced imaging. The appearance of a common flow artifact (misregistration artifact) on an usual acquisition is also reproduced. At last, a simulation of phase contrast on a realistic vessel geometry is presented. Those results include flow data based on theoretical flow model as well as complex numerical data obtained from Computational Fluid Dynamics (CFD).

CONCLUSION: The framework introduced provides an efficient and versatile tool for simulation of any MRI experience including physiological fluids with arbitrarily complex flow motion.

Keywords: MRI simulation, Bloch equations, angiography, complex flow, CFD, JEMRIS

Introduction

Since the princeps work of Bittoun et al. [1], MRI simulation has proven to be an effective tool for numerous research fields. Design of new pulse sequences, testing of physical models, development of new methods or even educational purposes [2] are the main applications usually cited. However, the simulation of realistic experiences supposes to take into account the effect of physiological circulating fluids, considering that blood flow can induce numerous artifacts and lead to misinterpretation. Furthermore, including flow motion into an MRI simulation is a necessary condition to study the specific field of angiographic techniques such as time-of-flight, contrast-enhanced angiography or phase-contrast velocimetry, and it can also be an efficient tool for exploration of perfusion with spin labeling techniques.

Considering this, several approaches were developed to simulate specifically the whole physical process of MR angiography coupled with Computational Fluid Dynamics (CFD) methods. Those techniques can be classified as Lagrangian [3], Eulerian [4] and mixed approaches [5], depending on the way to express and solve Bloch equations. However, the most advanced and disseminated MRI simulators to date are widely specialized in static tissues simulation and generally do not include a specific option for flow modeling. This is the case, e.g., for SIMRI [6], ODIN [7], POSSUM [8] and JEMRIS [9]. ODIN is specialized in the simulation of diffusion phenomena, based on Bloch-Torrey equations, while POSSUM focuses especially on fMRI. Both POSSUM and JEMRIS can take into account spins displacement involved in rigid body motion. A more recent software, MRISIMUL, is the only exception which shows the ability to simulate laminar flow motion from analytical velocity expression [10].

Therefore, most existing softwares are not intended to deal with complex flow data from CFD and they are mainly based on analytical time-discretized solutions of Bloch equations, which imposes some limitations on the MRI pulse-sequence and prohibits the use of complex RF waveforms and gradients. Thus, we aimed to develop a verstaile framework for MRI simulation that can deal with any pulse sequence and arbitrary complex flow pattern. A brief overview of the theoretical bases of MRI flow simulation is first presented. Then, the implementation

of a Lagrangian description of the flow in an existing software (JEMRIS) is described as an effective way to get a complete tool for angiographic experiences. The conditions to impose on the trajectories and the choice of parameters for physically realistic simulations are also introduced. The efficiency of this framework is then illustrated by presenting a set of results based on analytical velocity expressions, with the main three classical angiographic techniques: phase contrast (PC), time-of-flight (TOF) and contrast-enhanced imaging with contrast agent injection. The ability to reproduce a well-known flow artifact (misregistration artifact) is also demonstrated. Comparisons are established with some experimental acquisitions on a physical flow phantom. At last, a simulation of blood circulation in a realistic vein geometry with complex flow data from CFD is presented.

Theory

The approaches proposed to simulate angiographic images can be classified into Lagrangian, Eulerian and mixed methods.

Lagrangian approach

Lagrangian approach use the same method to describe flowing particles and static tissues [3]. To this end, the position of the isochromats is made variable:

$$\mathbf{r} = \mathbf{r}(t) \Rightarrow \quad \mathbf{B}(\mathbf{r}, t) = [\mathbf{G}(t).\mathbf{r}(t) + \Delta B(\mathbf{r}, t)].\mathbf{e_z} + \mathbf{B_1}(\mathbf{r}, t)$$

where $\mathbf{G}(t)$ is the gradient field, $\mathbf{r}$ is the isochromat position, $\Delta B(\mathbf{r}, t)$ is the field inhomogeneity due to off-resonance and non-uniform gradients, and $\mathbf{B_1}(\mathbf{r}, t)$ the RF pulse. The classical expression of Bloch equations is then solved individually for each isochromat to get the value of the macroscopic magnetization $\mathbf{M}(t)$ of the spin along its trajectory[1]:

$$\frac{d\mathbf{M}}{dt} = \gamma \mathbf{M} \times \mathbf{B} - \hat{\mathbf{R}}(\mathbf{M} - \mathbf{M_0}) \tag{1}$$

where $\mathbf{M}$ is the magnetization vector of the isochromat, $\mathbf{M_0}$ is the steady state value of magnetization, γ is the gyromagnetic ratio, $\mathbf{B}$ is the magnetic field and $\hat{\mathbf{R}}$ the relaxation matrix with T_1 and T_2 relaxation times.

$$\hat{\mathbf{R}} = \begin{pmatrix} 1/T_2 & 0 & 0 \\ 0 & 1/T_2 & 0 \\ 0 & 0 & 1/T_1 \end{pmatrix}$$

The Lagrangian approach is the most intuitive way to simulate flow motion, as it closely mimics the physical process of fluid circulation. Its main advantage is the ease of solving of Bloch equations, which are simple ordinary differential equations ODE. It is thus possible to implement analytical time discretized solutions in the algorithm for many simplified pulse-shape sequences. The independent treatment of each isochromat is also well-suited for parallelization by splitting the sample between multiple cores. Moreover, flowing particles do not need a specific process, compared to static tissues. Another asset is the possibility to easily simulate specific experiences with heterogeneous fluid interactions, such as contrast agent injection, by simply changing the relaxation time of the dynamic isochromats. As a counterpart, the main constraint of this method is the necessity to determine the individual particles trajectories, which add an additional step. Moreover, depletion or accumulation of spins can lead to signal blanks or peaks in the image if the flow is complex or turbulent.

Eulerian approach

Eulerian approach is based on a formalism inspired from fluid mechanics. Magnetization is hence considered as a field depending on space and time $\mathbf{M}(\mathbf{r}, t)$. Bloch equations are modified by inserting in Eq. (1) the Eulerian expression of the total particle derivative:

$$\frac{d\mathbf{M}}{dt} = \frac{\partial \mathbf{M}}{\partial t} + (\mathbf{V}.\nabla)\mathbf{M} \tag{2}$$

where $\mathbf{M}$ is the magnetization vector of the tissue and $\mathbf{V}$ is the velocity of the flowing spins. The Partial Derivative Equation (PDE) can then be solved on a mesh to get the value of magnetization on a discrete collection of points over the sample [4] [11].

The main advantage of this technique is that both Bloch and Navier-Stokes equations can be solved successively on the same mesh and then do not need a separated process. Moreover, there is no need to compute individual particles trajectories, which can be an expensive computational step. The main drawback is the complexity of PDE solving and its parallelization, which requires specific technical knowledge. Furthermore, the simulation of misregistration artifacts need some specific process with this approach.

Mixed approach

All methods proposing an intermediate solution beetwen both previous could be classified as "mixed" methods. For instance, some iterative approaches propose to calculate the value of magnetization in a collection of fixed points by separating Bloch evolution of the spin from fluid advection phenomena [5]. At each time step, Bloch equations are iterated on a fixed grid, and the value of magnetization is then translated to the neighboring points, proportionally to the local velocity. The main advantage of this physically intuitive method is that it avoid to calculate particles trajectories separately. As for Lagrangian methods, the equations are a simple ODE system. However, an additional step is required to consider the advection of magnetization due to spins motion.

Methods

Conventional MRI simulators have been highly developed over the last decades. Therefore, implementing a description of flow motion into an existing software is an efficient way to get a complete tool for virtual angiography. From this point of

[1] In this context, the terms "isochromat", "spin" and "particle" are used as synonymous.

view, JEMRIS is to date one of the most full-featured simulation platforms [9], based on a numerical solving of Bloch equations with the external library CVODE[2] and Adams-Moulton linear multistep method. This allows to reproduce any pulse-shape sequence with arbitrary complex gradients and RF waveforms, where no analytical solution is known, whereas simulators based on a time-discretized solution are generally limited to piecewise constant gradient fields and hard-pulse approximation. A comprehensive list of physical effects involved in the imaging process is also taken into account, such as off-resonance effects (including T2*), non-uniform gradients, parallel receive and transmit and the effect of rigid body motion.

The choice to implement a Lagrangian description of the flow into this software was the most obvious in regard of the existing code and the most suitable for parallel computing. The extensible structure of C++ allowed to add this feature without deep modification of the existing operating mode. A specific class was appended to allow the user to specify a trajectory for each flowing spin individually. With this new version, it thus became possible to describe complex flow motion while maintaining all the features inherited from the original software.

Dynamic isochromats settings

The description of the flow in terms of Lagrangian trajectories requires to fulfill some specific conditions for realistic simulations.

Trajectories format. Individual trajectories are described for each spin successively by specifying a discrete collection of positions over the pulse sequence. Intermediate positions are then determined by linear interpolation. No restriction is made on the timestep interval of the trajectories which is determined by the user depending on the desired level of precision in the flow description. The time interval need not be homogeneous and can be increased to describe precisely non-straight parts of the trajectories.

Continuous flow. To reproduce a continuous flow of particles, the vessel must be already filled at the beginning of the pulse sequence and a continuous seeding of isochromats is required during the whole experience. However, in the case of periodic flow due to heartbeat, the same trajectories can be reused periodically to reduce flow data volume. Moreover, in the case of sequences with long TR, one can also synchronize spins seeding to RF pulse to reduce the number of particles.

Isochromats density. To simulate MR signal with discretely distributed points, at least one isochromat per voxel is needed to get a consistent image of the sample. Moreover, it has been shown that at least two isochromats per voxel and direction are needed to get an error lower than 3,5% on the calculated signal, and that three isochromats per voxel and direction are needed to get an error lower than 1,5% [12]. For simulation of incompressible fluids, as well as for static tissues, the spatial interval between neighboring isochromats must incur few variations over space and time, to prevent depletion or accumulation of spins in a voxel:

$$\rho_{isochromats}(\mathbf{r}, t) \approx constant$$

where $\rho_{isochromats}(\mathbf{r}, t)$ is the density of static and dynamic isochromats at a given time and position. A too much irregular distribution of spins can, indeed, lead to artificial signal peaks or blanks in some regions, as the software does not intend to control the density of input flow trajectories and to correct potential inhomogeneities.

Besides, in the case of flow data from CFD to study complex vessel geometries, it can be difficult to get a set of trajectories preserving a uniform spatial distribution of spins. Indeed, previous studies on particle tracking suggest that even with highly resolved CFD mesh and high particles density, a uniform distribution of spins at inlet never remains perfectly uniform by flowing throughout a complex geometry [13]. Increasing the density of particles can reduce the effect of local inhomogeneities but will result in higher execution times. Therefore, seeding the entry of the geometry with a constant spatial step is a more efficient approach than a constant timestep, as a regular seeding over time leads to a depletion at the center of the vessel, in the regions of high velocities, and to an accumulation at the edges of the vessel. To achieve this, a paraboloidal distribution of spins can be used, proportional to the local velocity and to the time-seeding interval (Fig. 1).

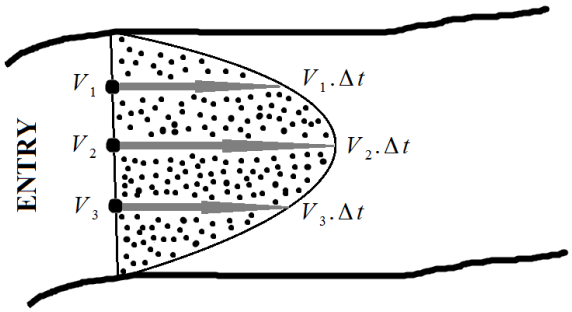

Figure 1: Paraboloidal seeding of the geometry, proportionally to the local velocity and to the time-seeding interval Δt, ensures an homogeneous density of particles at the center and at the edges of the vessel.

Spoiling gradients. Another restriction appears with spoiled pulse sequences resulting from the discrete spatial localization of the isochromats, which can lead to artificial spins refocusing and to unrealistic artifacts. Contrary to biological tissues with a continuous distribution of spins, a discrete distribution of isochromats can lead to constructive magnetization summation inside a voxel [14]. Some simulators workaround by calculating intravoxel magnetization gradients [7] or by nulling transversal magnetization artificially when a spoiling gradient is applied [10]. In the present framework, increasing the number of particles per voxel is a way to circumvent the problem, but results in higher execution times. Artificially reducing T_2

[2] http://computation.llnl.gov/projects/sundials

delay is also possible when its effect is not of crucial importance for the experience.

Total number of isochromats. For each acquisition with incompressible flow, the total number of dynamic isochromats $N_{dynamic}$ is given by:

$$N_{dynamic} = (V_{geometry} + Q \times T_{sequence}) \ / \ (\delta x.\delta y.\delta z)$$

where $V_{geometry}$ indicates the total inner volume of the vessels geometry, Q denotes the total inflow rate, $T_{sequence}$ is the total duration of the experience and $\delta x, \delta y, \delta z$ denote the mean spatial interval between neighboring isochromats.

Spins storage. Before they enter the region of interest (ROI), and after they leave it, dynamic spins can often be stored in a static place. Therefore, those particles must not disturb the rest of the image with spurious signal. The solution provided is to filter numerically the signal outside of the ROI. Thereupon, a tool for antenna design with adjustable spatial extent is natively proposed in the software.

Hardware implementation

JEMRIS proposes a parallel mode via MPI. Computation time greatly depends on the content of the pulse sequence and on CVODE module performances. Hence, there is no simple linear relation between computation time and pulse sequence duration, contrary to simulators based on analytical time-discretized solutions. The present simulations were performed on a supercomputer, with a few hundred of CPUs for each experience.

Experimental flow phantom

The experimental flow phantom was an hydrodynamic bench with a flexible tube inside and a rigid tube as return line, as shown on Fig. 2. The dimensions of the bench were 110 mm × 120 mm × 390 mm. The flexible tube had an inner diameter of 19 mm at rest and a thickness of 1,04 mm. The pipe wall reproduced compliance of an artery [15] (0,32%/mmHg) and was immersed in static water to avoid deformations effects from gravity. The rigid return line had an inner diameter of 22 mm.

For phase contrast experiences, Glycerol was injected in the flowing water to get a dynamic viscosity of $2,4.10^{-3}$ Pa.s, close to blood viscosity at 37°C and leading to laminar flow conditions. All experiences were carried out with steady flow and images were acquired on a 3T Siemens Magnetom Verio.

Misregistration artifact I

The standard misregistration artifact, or displacement artifact, is a well-known motion-induced artifact resulting in an error of location of the flowing spins on the image due to the motion of particles between phase encoding gradient and readout gradient [16]. For this simulation, a simplified model of in-plane plug flow was used, with uniform velocity $V_0 = 150$ mm/s and diameter of 20 mm, inclined by 45° in the plane of the slice. The distance between neighboring isochromats was 0,5 mm with a total number of 270 168 particles. The sequence

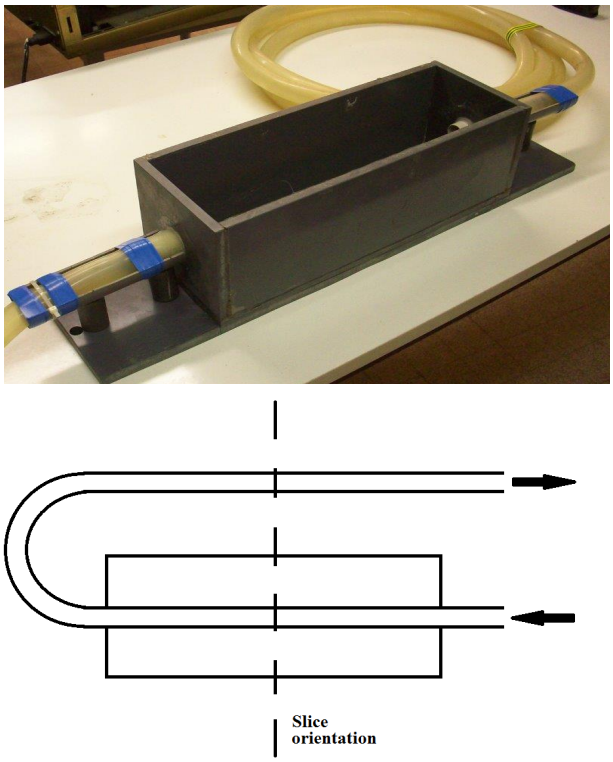

Figure 2: Top: Experimental flow phantom. The inner flexible tube is immersed in static water to avoid gravity effects. Bottom: Orientation of the slice for the angiographic experiences.

used was gradient echo, the 2D acquisition matrix was 64×64, the pixel size was 1,56 mm × 1,56 mm, TE was 120 ms, TR was 300 ms and NEX was 1. The time interval between phase encoding and readout was set to 100 ms.

Misregistration artifact II

Another specific misregistration artifact was also simulated, which appears with a vessel going through a 2D-slice with an oblique angle [17]. Thus, blood excited during the slice selection will continue its motion and its final position will be encoded during phase and readout gradients. Displacement in the readout direction is directly proportional to the TE delay, which is not necessary the case for the classical misregistration artifact. For a straight tube with steady flow inclined by the angle α to the slice in the readout direction, the apparent displacement Δx of a particle with constant velocity V_0 is given by:

$$\Delta x = V_0.TE.sin(\alpha)$$

For this experience, the experimental hydraulic flow rate was 114,8 mL/s in a tube of 20 mm in diameter, with non-laminar flow conditions, close to plug flow. The tube was inclined by $30,2°$ in the readout direction. Experimental FOV was 246 × 184,5 mm, 2D acquisition matrix was 576 × 432 (i.e., pixel size was 0,42 mm × 0,42 mm), slice thickness was 5 mm, TR

was 66 ms, RF pulse angle was 15°, NEX was 32 and flow compensation mode was active.

For the simulation, a simplified model of plug flow was used, with uniform velocity $V_0 = 366$ mm/s in a tube with an inner diameter of 20 mm, leading to a flow rate of 114,8 mL/s. The tube was inclined by $30,2°$ in the readout direction. The distance between neighboring isochromats was 1 mm in the direction of the flow and 0,39 mm in the radial direction, leading to a total of 3 808 000 particles. The sequence used was a classical spoiled gradient echo. The 2D acquisition matrix was 71×64, the pixel size was 0,78 mm × 0,78 mm, the slice thickness was 5 mm, TR was 66 ms and NEX was 1.

Time-of-flight sequence

The implementation of a Lagrangian description of flow also allows to reproduce angiographic acquisitions including both static structures and flow. To this end, the experimental flow phantom was first modeled with the appropriate trajectories. The same flow data were then used as input to simulate the main three angiographic sequences (TOF, PC and contrast-enhanced MRA). A steady laminar flow in straight tubes was considered, with velocities following the Poiseuille law. The flow rate was 15 mL/s and the internal diameter was set to 20 mm for the internal tube and 22 mm for the external one.

For the 2D TOF sequence, a short TR of 12 ms and TE of 8 ms were taken, with a full flip angle of 90° in order to saturate the signal from static spins and to favor entry effect. The k-space matrix was 83×115 and the pixel size was 1,56 mm × 1,56 mm. The T_1 relaxation time of the dynamic spins was set to 1 154 ms, according to the experimental values measured for the water-glycerol mixture. The T_1 for the static spins of the phantom (static water), was set to 2 885 ms. A total of 1 354 810 spins was used for this simulation.

Contrast agent injection

Contrast agent injection can be directly simulated with the same flow data as previously by reducing the T_1 delay of the dynamic particles. Thus, for this simulation, T_1 was set to 154 ms for the flow and 2 885 ms for the static water. A 2D T_1-weighted sequence was used with TR of 5 ms, TE of 2 ms and flip angle of 45°. The k-space matrix was 83×115 and the pixel size was 1,56 mm × 1,56 mm.

Phase contrast I

The framework enables to simulate measurements of flow velocity and, optionally, acceleration, based on phase contrast pulse sequences. 1D-velocity encoding was performed here for a flow going through the slice, by adding a trapezoidal bipolar gradient on a classical gradient echo pulse sequence. Sequence was then run twice, with opposite bipolar gradient sign and velocity map was then obtained by phase subtraction.

Simulations were compared to experimental phase contrast images acquired on the physical flow phantom under similar conditions. The experimental hydraulic flow rate was 15 mL/s, the matrix was 512×384, the pixel size was 0,39 mm × 0,39 mm, slice thickness was 0,1 mm, TR was 55,1 ms, TE was 8,3 ms, RF pulse angle was 15°, NEX was 1 and Venc was 200 mm/s.

The simulated flow rate was 15 mL/s in both tubes, the 2D matrix was 461×333, the pixel size was 0,39 mm × 0,39 mm, the slice thickness was 2,5 mm and maximum velocity encoding Venc was 200 mm/s. TE was 10 ms, TR was 16 ms and RF pulse angle was 15°. A reduced TR was chosen compared to the experimental data in order to reduce the experience duration and consequently the number of isochromats. The same way, a larger slice thickness was used in the simulation to get a sufficient number of dynamic particles in the slice during the whole acquisition, without increasing the density of isochromats per mm^3. Thus, the inter-spins distance was set to 0,3 mm in the plane of the slice and 1,5 mm normally to the slice, leading to a total of 2 069 943 isochromats.

Phase contrast II

Previous simulations were performed with analytical flow models, therefore a simulation of blood circulation in a realistic jugular vein geometry obtained from real MRI acquisitions is also presented. Velocity data were generated by solving Navier-Stokes equations on a mesh with CFD methods [18]. The trajectories were then computed with particle tracking methods on the resulting mesh. The geometry was initially filled with a random distribution of particles, with a mean distance of 0,15 mm between neighboring isochromats. Steady flow conditions were considered and the same trajectories were reused periodically at each TR to limit the number of particles. The 2D k-space matrix of the sequence was 32×32, the pixel size was 0,39 mm × 0,39 mm, the slice thickness was 2 mm, TE was 8 ms, TR was 12 ms, RF pulse angle was set to 15° and 1D velocity encoding was carried out normally to the slice with Venc = 350 mm/s.

Results

Parallel processing allowed time saving to deal with large samples containing high number of isochromats, as summarized in Table 1 for each experience. The results for the classical in-plane misregistration artifact are shown on Fig. 3. As expected, flow displacement is clearly visible with the uncorrected sequence. The second misregistration artifact is shown on Fig. 4, depending on TE delay, with comparison of simulation with experimental data. Table 2 shows a good agreement for the displacement magnitude between theoretical and measured values. Simulations of the flow phantom with the main three angiographic techniques are presented on Fig. 5 and Fig. 6. First, Fig. 5 shows anatomical acquisitions simulated with TOF and contrast agent injection. As expected, only the signal inside both tubes is clearly contrasted on those images, compared with a classical gradient echo simulation. Then, Fig. 6 illustrates the possibility to carry out some velocimetric measurements on the flow by comparing experimental and simulated phase contrast images of the flow phantom. The velocities measured are in good agreement with the values used as input. This first validates the ability of the framework to reproduce simple flow models. Finally, the phase contrast simulation

Simulation	Matrix lines	Isochromats	CPU	Calculation [min]	Calculation [ms × CPU / isocromat]
Misregistration 1	64	270 168	100	3	67
Misregistration 2	64	3 808 000	180	62	176
TOF	83	1 354 810	150	20	133
Contrast-enhanced	83	1 354 810	100	31	137
Phase contrast	333	2 069 943	300	330	2870
Phase contrast vein	32	1 479 905	200	86	697

Table 1: Computation times for each simulation experience.

of blood circulation in the realistic vein geometry is shown on Fig. 7. Velocities measured are also in good agreement with input flow data, highlighting the efficiency of the framework to simulate complex flow data from CFD.

TE (ms)	Theory (mm)	Simulation (mm)	Experiment (mm)
40	11	10,9 ± 0,8	11,1 ± 0,9
50	9,2	9,4 ± 0,8	9,0 ± 0,9
60	7,4	7,0 ± 0,8	7,3 ± 0,9

Table 2: Apparent displacement magnitude of the misregistration artifact in the readout direction for different TE values.

Discussion and conclusion

An open-source and extensible work for high performance MRI simulation of any experiment including fluid particles was presented. This covers, *inter alia*, the field of angiographic acquisitions as well as the study of flow effects on classical pulse sequences.

The Lagrangian approach is well-suited for parallel computing and does not require specific technical knowledge, which allows to carry out realistic simulations of large samples including both static tissues and arbitrarily complex flow motion. As it closely mimics the physical process of fluid circulation, the injection of some specific substances such as contrast agent can be directly reproduced. Simulations can take as entry synthetic flow data from theoretical flow models as well as numerical flow data from CFD, for simulation of blood flow in realistic complex vessels geometry. Results presented in 2D with steady flow can be easily extended to 3D and pulsatile flow, e.g. for the simulation of a full cerebral vasculature, with the possibility to reuse the same trajectories periodically to reduce input data.

Other simulators have already proposed some results for flow simulation, but they generally only concern data from analytical velocity expression [10] or they only deal with a very specific type of acquisition. Some of them are exclusively centered on flow simulation study [3, 4, 5] or only reproduce a specific type of pulse sequence [19]. Contrarily to those specialized codes, choosing to extend a pre-existing high performance MRI simulator allows for getting very few limitations. Moreover, no restriction is imposed on flow timestep precision as JEMRIS kernel is based on a numerical solving of Bloch equations, contrary to other simulators commonly based on a time-discretized analytical solution. Parallelization allows to perform simulations of large samples with reduced time consumption. All those characteristics lead to a tool offering a very high degree of versatility.

Combining this work with all the existing possibilities of the original software, JEMRIS is to date one of the most efficient and versatile tools for simulation of any complex MRI experience.

Acknowledgements

Thanks are due to JEMRIS developers to provide this complete tool to the MRI community.

Experimental images were acquired with guidance from the members of the ICube imaging platform at University of Strasbourg, CNRS, ICube, FMTS, Strasbourg, France.

Particle tracking was made in collaboration with Alexandre Ancel from IRMA at University of Strasbourg and Simon Garnotel from BioFlowImage at University Picardie Jules Verne.

Parallel computing was performed with ROMEO HPC center, hosted by the University of Reims Champagne-Ardenne (https://romeo.univ-reims.fr).

This research was funded by the French *Agence Nationale de la Recherche* (VIVABRAIN project, Grant Agreement ANR-12-MONU-0010).

References

[1] J. Bittoun, J. Taquin, M. Sauzade, A computer algorithm for the simulation of any nuclear magnetic resonance (NMR) imaging method, Magnetic Resonance Imaging 2 (2) (1984) 113–120.

[2] L. Hanson, A graphical simulator for teaching basic and advanced MR imaging techniques, Radiographics 27 (6) (2007) e27.

[3] I. Marshall, Computational simulations and experimental studies of 3D phase-contrast imaging of fluid flow in carotid bifurcation geometries, Journal of Magnetic Resonance Imaging 31 (4) (2010) 928–934.

[4] S. Lorthois, J. Stroud-Rossman, S. Berger, L.-D. Jou, D. Saloner, Numerical simulation of magnetic resonance angiographies of an anatomically realistic stenotic carotid bifurcation, Annals of Biomedical Engineering 33 (3) (2005) 270–283.

[5] K. Jurczuk, M. Kretowski, J.-J. Bellanger, P.-A. Eliat, H. Saint-Jalmes, J. Bezy-Wendling, Computational modeling of MR flow imaging by the lattice Boltzmann method and Bloch equation, Magnetic Resonance Imaging 31 (7) (2013) 1163–1173.

[6] H. Benoit-Cattin, G. Collewet, B. Belaroussi, H. Saint-Jalmes, C. Odet, The SIMRI project: A versatile and interactive MRI simulator, Journal of Magnetic Resonance 173 (1) (2005) 97–115.

[7] T. H. Jochimsen, A. Schafer, R. Bammer, M. E. Moseley, Efficient simulation of magnetic resonance imaging with Bloch-Torrey equations using intra-voxel magnetization gradients, Journal of Magnetic Resonance 180 (1) (2006) 29–38.

[8] I. Drobnjak, D. Gavaghan, E. Sli, J. Pitt-Francis, M. Jenkinson, Development of a functional magnetic resonance imaging simulator for modeling realistic rigid-body motion artifacts, Magnetic Resonance in Medicine 56 (2) (2006) 364–380.

[9] T. Stocker, K. Vahedipour, D. Pflugfelder, N. J. Shah, High-performance computing MRI simulations, Magnetic Resonance in Medicine 64 (1) (2010) 186–193.

[10] C. Xanthis, I. Venetis, A. Aletras, High performance MRI simulations of motion on multi-GPU systems, Journal of Cardiovascular Magnetic Resonance 16 (1) (2014) 48.

[11] L. D. Jou, D. Saloner, A numerical study of magnetic resonance images of pulsatile flow in a two dimensional carotid bifurcation: A numerical study of MR images, Medical Engineering & Physics 20 (9) (1998) 643–652.

[12] P. Shkarin, R. G. S. Spencer, Time domain simulation of Fourier imaging by summation of isochromats, Imaging Systems and Technology 8 (1997) 419–426.

[13] M. Tambasco, D. A. Steinman, On assessing the quality of particle tracking through computational fluid dynamic models, Journal of Biomechanical Engineering 124 (2) (2002) 166–175.

[14] I. Marshall, Pulse sequences for steady-state saturation of flowing spins, Journal of Magnetic Resonance 133 (1) (1998) 13–20.

[15] M. Stevanov, J. Baruthio, B. Eclancher, Fabrication of elastomer arterial models with specified compliance, Journal of Applied Physiology 88 (4) (2000) 1291–1294.

[16] I. Marshall, Simulation of in-plane flow imaging, Concepts in Magnetic Resonance 11 (6) (1999) 379–392.

[17] T. C. Larson, W. M. Kelly, R. L. Ehman, F. W. Wehrli, Spatial misregistration of vascular flow during MR imaging of the CNS: Cause and clinical significance, American Journal of Neuroradiology 11 (5) (1990) 1041–1048.

[18] O. Miraucourt, O. Génevaux, M. Szopos, M. Thiriet, H. Talbot, S. Salmon, N. Passat, 3D CFD in complex vascular systems: A case study, in: Biomedical Simulation, no. 8789 in Lecture Notes in Computer Science, 2014, pp. 86–94.

[19] S. Petersson, P. Dyverfeldt, R. Gardhagen, M. Karlsson, T. Ebbers, Simulation of phase contrast MRI of turbulent flow, Magnetic Resonance in Medicine 64 (4) (2010) 1039–1046.

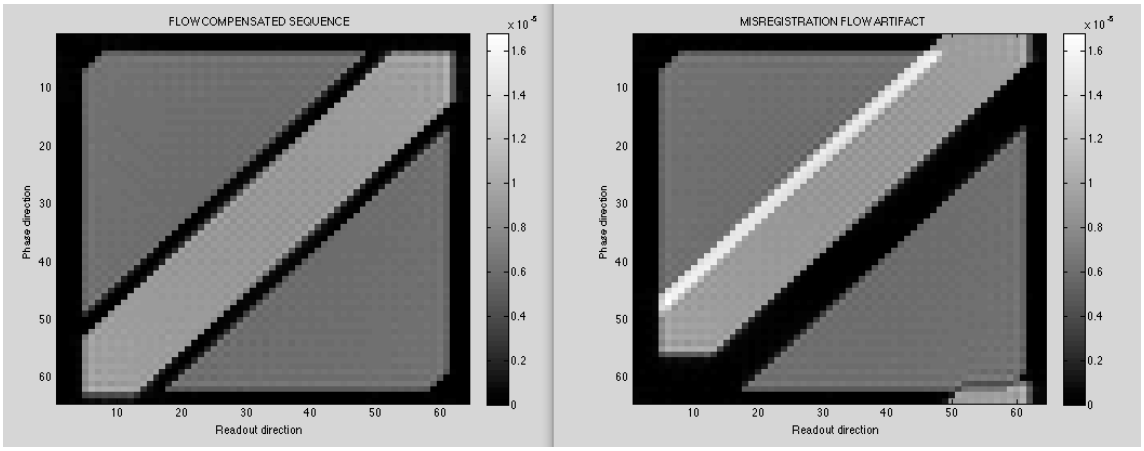

Figure 3: Misregistration artifact. JEMRIS simulation of a standard displacement artifact. Left: With flow-corrected pulse-sequence, the flow is normally located in the vessel. Right: With uncorrected pulse sequence, time delay between phase encoding and readout lead to an error in the position of the flow. An area of hypersignal appears when the signal of the flowing spins superimposes with that of static spins.

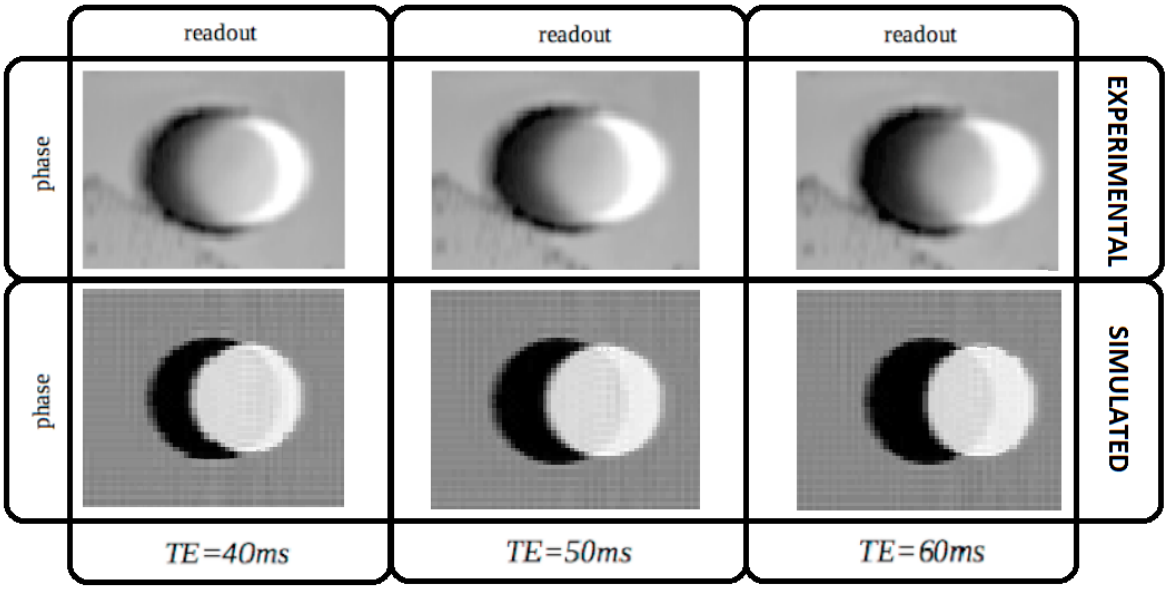

Figure 4: Misregistration artifact. Comparison between JEMRIS simulations and experimental images of displacement artifact in the readout direction, with oblique flow through the slice, for various TE delays. Simulation was made with a simplified model of plug flow to account for the non-laminar aspect of the experimental data.

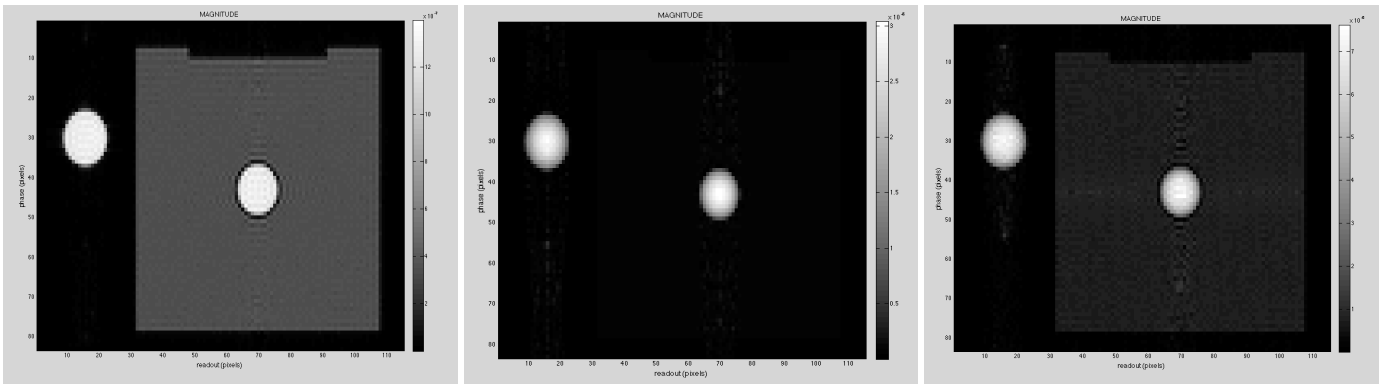

Figure 5: Simulation of various angiographic acquisitions on a physical flow phantom. Left: Simple gradient echo acquisition with $TR = 12$ ms, $TE = 8$ ms, $T2 = 50$ ms and RF angle set to 15°. The flow in both tubes is clearly contrasted due to entry effect. Middle: Time-of-flight acquisition on the phantom with the same physical parameters as previously. Right: Simulation of contrast-enhanced angiography with T_1-weighted sequence. Gadolinium injection is simulated by simply reducing T_1 value of the dynamic isochromats.

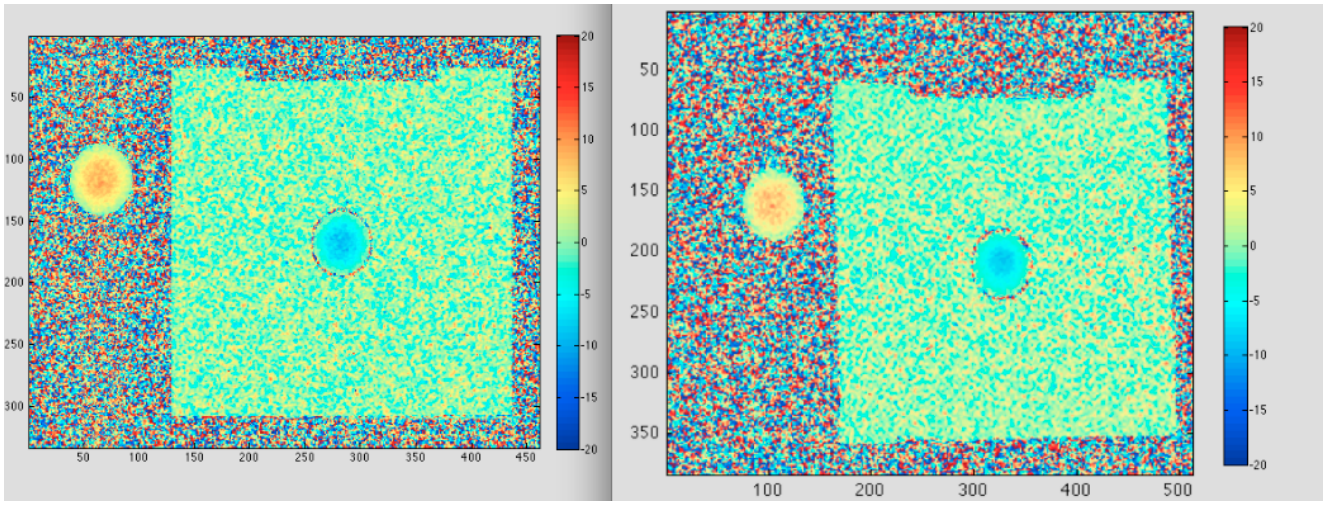

Figure 6: Phase contrast velocimetry on a physical flow phantom. Left: JEMRIS simulation based on a modelling of the phantom with synthetic flow data based on Poiseuille law. Right: Experimental image. At the center of both images, flexible tube with steady laminar flow, immersed in static water. On the left of the images, return line with steady laminar flow. The gradient of the Poiseuille law is visible in both tubes.

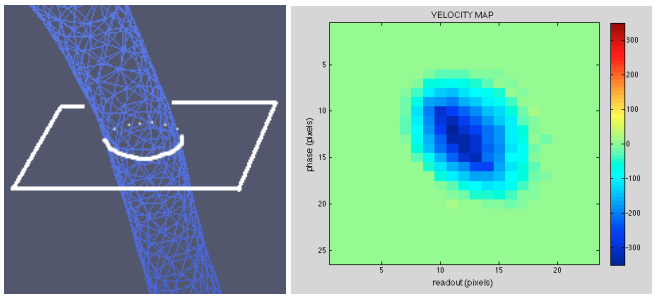

Figure 7: Simulation of phase contrast velocimetry on a jugular vein. Original velocities were obtained with CFD methods on a complex vein geometry from real MRI data. Trajectories were then computed numerically with particle seeding on the CFD mesh. Left: CFD mesh with slice orientation. Right: Simulated phase contrast image (background noise was filtered with the corresponding magnitude image).